Geophysical Research Letters

Supporting Information for

Where are white roofs more effective in cooling the surface?

Linying Wang[1], Maoyi Huang[2†], and Dan Li[1*]

[1]Department of Earth and Environment, Boston University, Boston, MA 02215, USA

[2]Atmospheric Sciences and Global Change Division, Pacific Northwest National Laboratory, P.O. Box 999, Richland, WA 99352, USA

[†]Now at Office of Science and Technology Integration, National Weather Service, National Oceanic and Atmospheric Administration, Silver Spring, MD 20910, USA

Contents of this file

Text S1

Figures S1 to S8

Tables S1 to S2

Introduction

This supporting information contains a description of the surface energy balance (SEB) model to quantify the effectiveness of cool roofs, defined as the reduction of roof surface temperature per unit increase of roof albedo ($\Delta T_s/\Delta\alpha$), Figures S1 to S8 and Tables S1 to S2.

Text S1. A Surface Energy Balance Model

To understand how the roof surface temperature responds to increases in albedo, we use a surface energy balance model (Bateni & Entekhabi, 2012), which starts with the surface energy balance equation for the roof, as follows:

$$R_n = S_{in}(1-\alpha) + \varepsilon L_{in} - \varepsilon\sigma {T_s}^4 = H + LE + G \quad \text{(S1)}$$

where R_n is the net radiation (W m^{-2}); S_{in} and L_{in} are the incoming shortwave (W m^{-2}) and longwave radiation (W m^{-2}), respectively; α and ε are the roof albedo and emissivity, respectively; H and LE are the sensible (W m^{-2}) and latent heat fluxes (W m^{-2}), respectively; $\varepsilon\sigma {T_s}^4$ is the outgoing longwave radiation (W m^{-2}) where σ is the Stefan-Boltzmann constant (W m^{-2} K^{-4}) and T_s is the roof surface temperature (K). G is the heat flux into the roof substrate (W m^{-2}), which is called ground heat flux in our paper following the convention.

Connecting H and LE with surface temperature through the aerodynamic resistance (r_a, s m^{-1}) and evaporation efficiency (β) concepts (Garratt, 1992) gives:

$$H = \frac{\rho c_p (T_s - T_a)}{r_a} \quad \text{(S2)}$$

$$LE = \beta \frac{\rho L_v (q_s^*(T_s) - q_a)}{r_a} \quad \text{(S3)}$$

where ρ is the air density (kg m^{-3}), c_p is the specific heat of air at constant pressure (J kg^{-1} K^{-1}), L_v is the latent heat of vapourization (J kg^{-1}), T_a is the air temperature (K), $q_s^*(T_s)$ is the saturated specific humidity at the surface temperature (kg kg^{-1}), and q_a is the air specific humidity (kg kg^{-1}).

The connection between G and surface temperature is achieved by using the force-restore method (Dickinson, 1988), which describes the evolution of the surface temperature can be expressed as the sum of the forcing term and a restoring term,

$$\frac{dT_s}{dt} = \frac{\sqrt{2\omega}}{\mu} G - \omega(T_s - \overline{T}) \tag{S4}$$

where μ is the thermal admittance of the roof (J m^{-2} K^{-1} s$^{-1/2}$), which is further determined by the volumetric heat capacity (c, J m^{-3} K^{-1}) and thermal conductivity (λ, W m^{-1} K^{-1}) of the roof though $\mu = \sqrt{c\lambda}$, ω is the principal diurnal frequency (s^{-1}), and $\overline{T}$ is the deep ground temperature (in our case $\overline{T}$ can be viewed as the temperature of the building interior, K).

Substituting Eqs. S1 to S3 into S4 yields

$$\begin{aligned}\frac{dT_s}{dt} = \frac{\sqrt{2\omega}}{\mu}\Big(S_{in}(1-\alpha) + \varepsilon L_{in} - \varepsilon\sigma {T_s}^4 - \frac{\rho C_p(T_s - T_a)}{r_a} \\ - \beta\frac{\rho L_v(q_s^*(T_s) - q_a)}{r_a}\Big) - \omega(T_s - \overline{T})\end{aligned} \tag{S5}$$

Note that the outgoing longwave radiation and saturated specific humidity are non-linear functions of surface temperature. To proceed, we linearize the outgoing longwave radiation and saturated specific humidity at air temperature, which yields:

$$\begin{aligned}\frac{dT_s}{dt} = \frac{\sqrt{2\omega}}{\mu}\Bigg(S_{in}(1-\alpha) + \varepsilon L_{in} + 3\varepsilon\sigma {T_a}^4 - 4\varepsilon\sigma {T_a}^3 T_s - \frac{\rho c_p(T_s - T_a)}{r_a} \\ - \beta\frac{\rho L_v}{r_a}\left(q_a^*(T_a) + \left.\frac{dq^*}{dT}\right|_{T_a}(T_s - T_a) - q_a\right)\Bigg) - \omega(T_s - \overline{T})\end{aligned} \tag{S6}$$

or

$$\frac{dT_s}{d\tau} = -\left(\frac{\rho c_p}{r_a} + 4\varepsilon\sigma {T_a}^3 + \mu\sqrt{2\omega} + \frac{\rho c_p}{r_a}\beta\frac{\delta}{\gamma}\right)T_s + Q' \tag{S7}$$

where

$$\tau = \frac{t}{\mu/\sqrt{2\omega}} \tag{S8}$$

$$\delta = \left.\frac{de^*}{dT}\right|_{T_a} \tag{S9}$$

$$\gamma = \frac{c_p P_a}{0.622 L_v} \tag{S10}$$

$$Q' = S_{in}(1-\alpha) + \varepsilon L_{in} + 3\varepsilon\sigma {T_a}^4 + \frac{\rho c_p}{r_a}T_a - \beta\frac{\rho L_v}{r_a}q_a^*(T_a) + \frac{\rho c_p}{r_a}\beta\frac{\delta}{\gamma}T_a + \beta\frac{\rho L_v}{r_a}q_a + \mu\sqrt{\frac{\omega}{2}}\bar{T} \tag{S11}$$

Here e^* refers to saturated water vapor pressure (Pa), which is only a function of temperature according to the Clausius-Clapeyron relation and γ is the Psychometric constant (Pa K^{-1}) (Brutsaert, 1982). We can further simplify the above equation as:

$$\frac{dT_s}{d\tau} = -\frac{T_s}{f} + Q' \tag{S12}$$

where

$$f = \frac{1}{\frac{1}{r_a'} + \frac{1}{r_o'} + \frac{1}{r_g'} + \frac{1}{r_e'}} \tag{S13}$$

$$r_a' = \frac{r_a}{\rho c_p} \tag{S14}$$

$$r_o{}' = \frac{1}{4\varepsilon\sigma {T_a}^3} \tag{S15}$$

$$r_g{}' = \frac{1}{\mu\sqrt{\frac{\omega}{2}}} \tag{S16}$$

$$r_e{}' = \frac{r_a}{\rho c_p \beta\delta/\gamma} \tag{S17}$$

The solution for the above equation is

$$T_s = T_s(0)e^{-\tau/f} + Q'f \tag{S18}$$

where $T_s(0)$ indicates the initial condition for roof surface temperature (K). The first part of solution is the time-dependent solution, which results from the time-dependence of surface temperature in the force-restore method, and the second part of the solution is the steady-state solution.

Assuming that the only difference between cool and regular roofs is the albedo, namely, cool and regular roofs share the same atmospheric forcing (e.g., incoming shortwave and longwave radiation, air temperature, air specific humidity, pressure, wind speed), building interior temperature, and other biophysical properties such as emissivity, thermal admittance, and aerodynamic features that affect the aerodynamic resistance, one can see that the only difference between the solution for cool roof and that for regular roof is the steady-state solution. Hence, we can express the surface temperature difference between cool and regular roofs as

$$\Delta T_s = \Delta Q'f = -S_{in}\Delta\alpha f \tag{S19}$$

or

$$\frac{\Delta T_s}{\Delta \alpha} = -S_{in} f \tag{S20}$$

which is Eq. (2) in the main text.

While the derivation leading to Eq. (S20) is exact under the assumptions elaborated earlier for any time instant in a continuous time domain, in practice the application of Eq. (S20) inevitably involves discretizing the time domain and some sort of time averaging. For example, when only the time averaged (e.g., daily mean or 3-hourly mean) values of the resistances and incoming shortwave radiation are provided, we have to further assume that the time averaged values can be used in Eq. (S20), as follows:

$$< \frac{\Delta T_s}{\Delta \alpha} > \approx - < S_{in} > \frac{1}{< \frac{1}{r'_a} > + < \frac{1}{r'_o} > + < \frac{1}{r'_g} > + < \frac{1}{r'_e} >} \tag{S21}$$

where the bracket indicates the time average. The approximation sign emerges due to the nonlinearity in Eq. (S20). More subtly, the discretization of the time domain actually prevents us from assuming that the cool roof and regular roof have the same initial condition for each averaging interval. The time-dependent solution of Eq. (S18) needs to be re-considered, especially for short averaging intervals. These complexities are not further pursued in our study.

It is important to highlight the differences between the surface energy balance model presented here and a growing number of models recently used for attributing surface temperature anomalies induced by land-use and land-cover changes (Burakowski et al., 2018; Chen & Dirmeyer, 2016; Lee et al., 2011; Li et al., 2019; Li & Wang, 2019; Liao et al., 2018; Luyssaert et al., 2014; Moon et al., 2020; Rigden & Li, 2017; Wang et al., 2019; Zhao et al., 2014). The key difference is that nearly all other models treat the ground heat

flux as an external forcing (similar to the treatment of ground heat flux in the famous Penman equation) while the model presented here treats the ground heat flux as a function of the internal variable: surface temperature. This is accomplished through the use of the force-restore model. This new treatment of the ground heat flux allows us to avoid the need to obtain the ground heat flux *a prior*. More importantly, the role of thermal admittance now emerges naturally. These advantages are why we choose this model in this study. However, by employing a model for the ground heat flux, its performance will then inevitably affect the fidelity of the final model for surface temperature (Eq. S20). Another difference, which has been discussed extensively in Rigden and Li (2017), is the parameterization of latent heat flux. Here the evaporation efficiency concept is used while the surface resistance concept was used in many previous studies (Liao et al., 2018; Moon et al., 2020; Wang et al., 2019). In some other studies (Lee et al., 2011; Zhao et al., 2014), the Bowen ratio was used. The surface relative humidity has also been used (Li & Wang, 2019). Different parameterizations are used in different studies as they offer different levels of analytical tractability and compatibility with data driving these models, which can either come from observations or more complicated numerical models. A comprehensive review and comparison of different models are beyond the scope of this study.

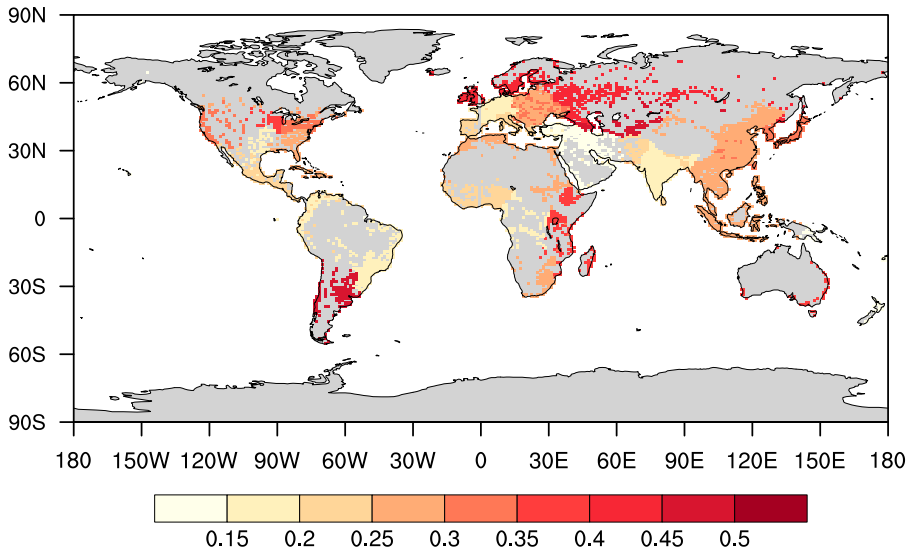

106

107 **Figure S1.** The spatial pattern of snow-free albedo for regular roofs. Only grid cells with

108 more than 0.1% of urban land are shown.

109

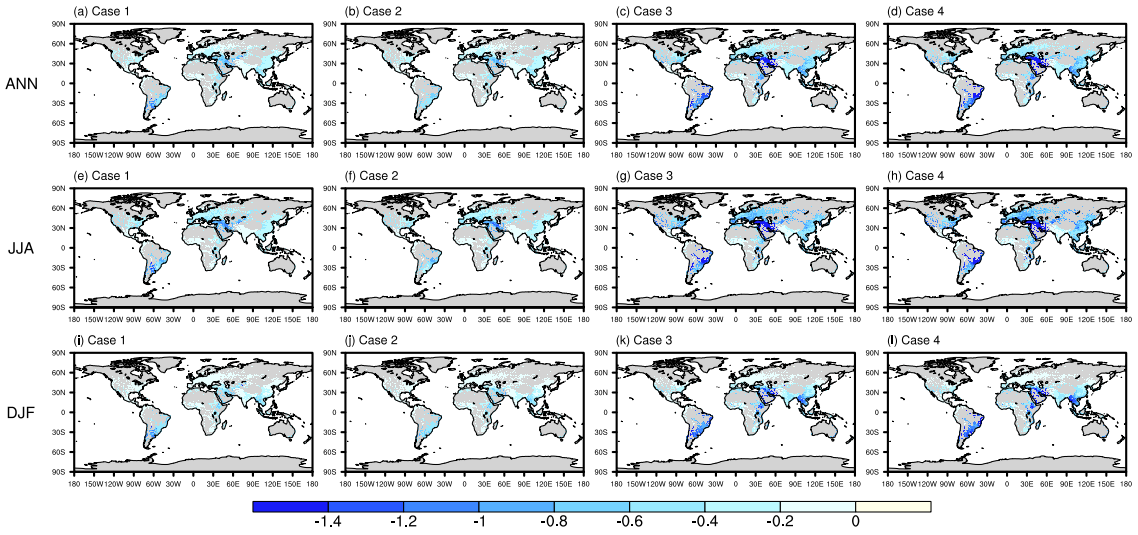

Figure S2. The differences in terms of near-surface air temperature between (a, e, i) Case 1, (b, f, j) Case 2, (c, g, k) Case 3, (d, h, l) Case 4 and CTL. (a-d) are the annual daily mean (ANN), (e-h) are the JJA daily mean, and (i-l) are the DJF daily mean over 20 years (1991-2010). Only grid cells with more than 0.1% of urban land are shown.

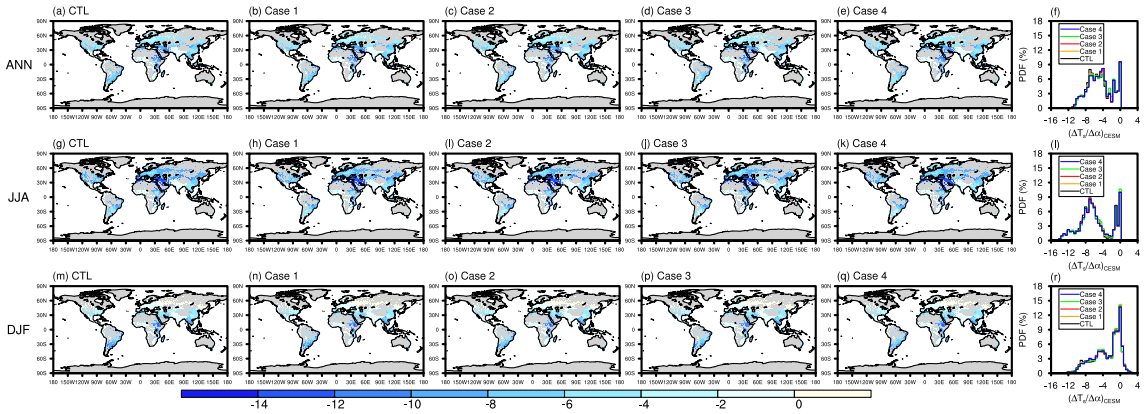

116

117 **Figure S3.** Roof surface temperature reduction in response to roof albedo increase (unit:
118 K) computed from land-only simulations: (a, g, m) CTL; (b, h, n) Case 1; (c, i, o) Case 2;
119 (d, j, p) Case 3; (e, k, q) Case 4. Also shown are the probability density functions (f, l, r).
120 (a-f) are the annual daily mean (ANN), (g-l) are the JJA mean, and (m-r) are the DJF mean
121 results over 20 years (1991-2010). Only grid cells with more than 0.1% of urban land are
122 shown.

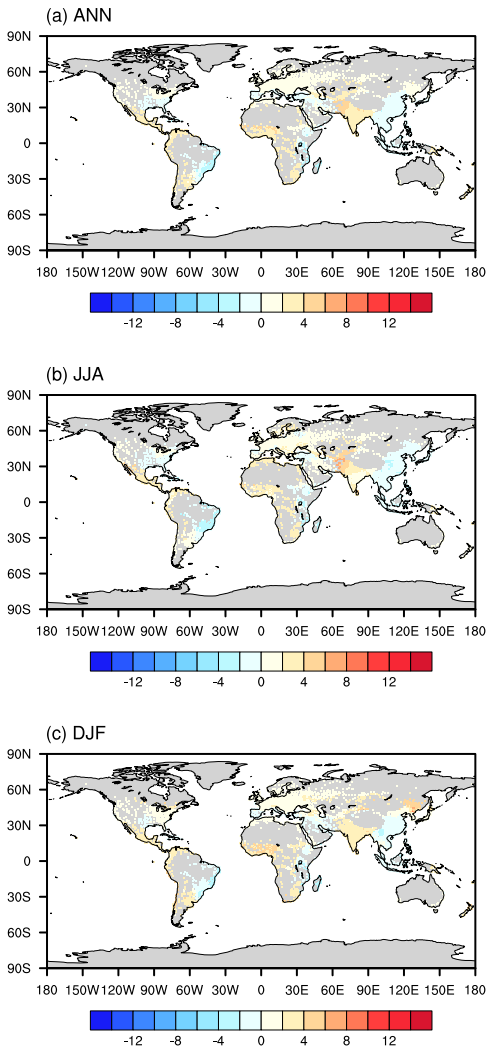

Figure S4. The difference between $(\Delta T_s/\Delta\alpha)_{CESM}$ and $(\Delta T_s/\Delta\alpha)_{SEB}$, unit: K. (a) is the annual daily mean (ANN), (b) is the JJA daily mean, and (c) is the DJF daily mean results over 20 years (1991-2010). The results shown here are from the Case 4 (100% cool roof with albedo value of 0.7). Only grid cells with more than 0.1% of urban land are shown.

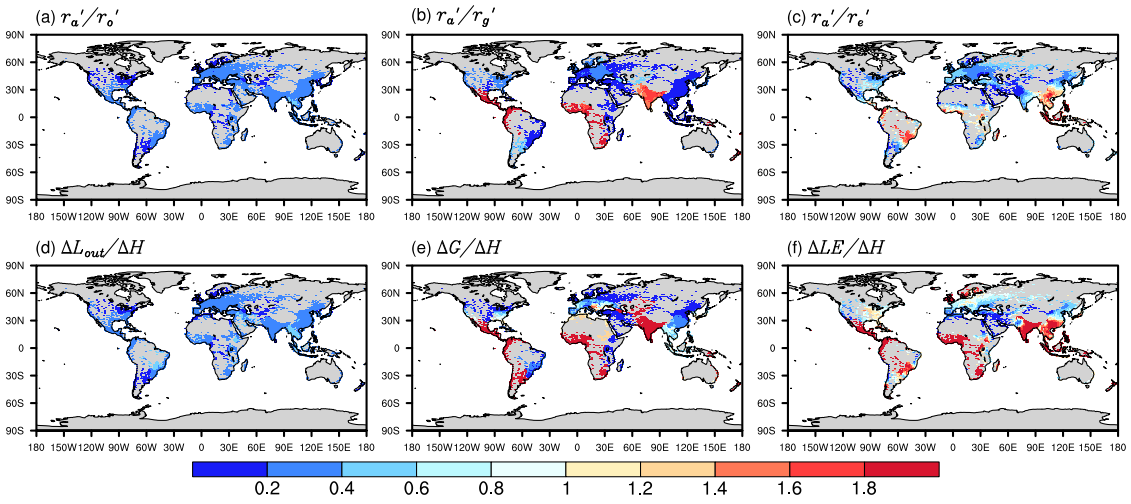

128

129 **Figure S5.** The ratios of efficiencies for (a) outgoing longwave radiation, (b) ground heat
130 flux, and (c) latent heat flux to the efficiency for sensible heat flux, and the corresponding
131 ratios of changes in (d) outgoing longwave radiation, (e) ground heat flux, and (f) latent
132 heat flux to changes in sensible heat flux in response to roof albedo increase. The results
133 are the ANN daily mean over 20 years (1991-2010) from the Case 4 (100% cool roof with
134 albedo value of 0.7). Only grid cells with more than 0.1% of urban land are shown.

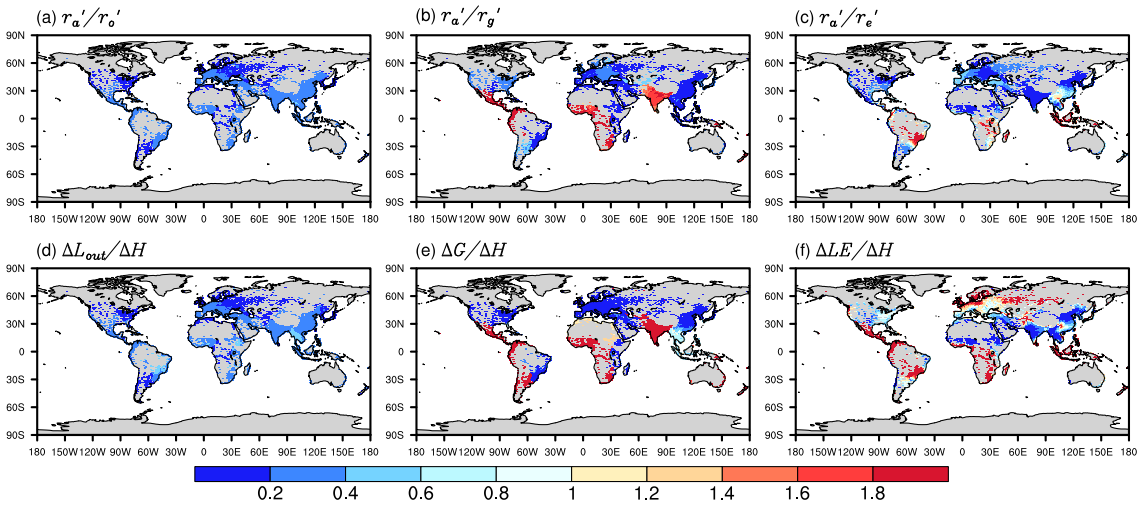

135

136 **Figure S6.** The ratios of efficiencies for (a) outgoing longwave radiation, (b) ground heat
137 flux, and (c) latent heat flux to the efficiency for sensible heat flux, and the corresponding
138 ratios of changes in (d) outgoing longwave radiation, (e) ground heat flux, and (f) latent
139 heat flux to changes in sensible heat flux in response to roof albedo increase. The results
140 are the DJF daily mean over 20 years (1991-2010) from the Case 4 (100% cool roof with
141 albedo value of 0.7). Only grid cells with more than 0.1% of urban land are shown.

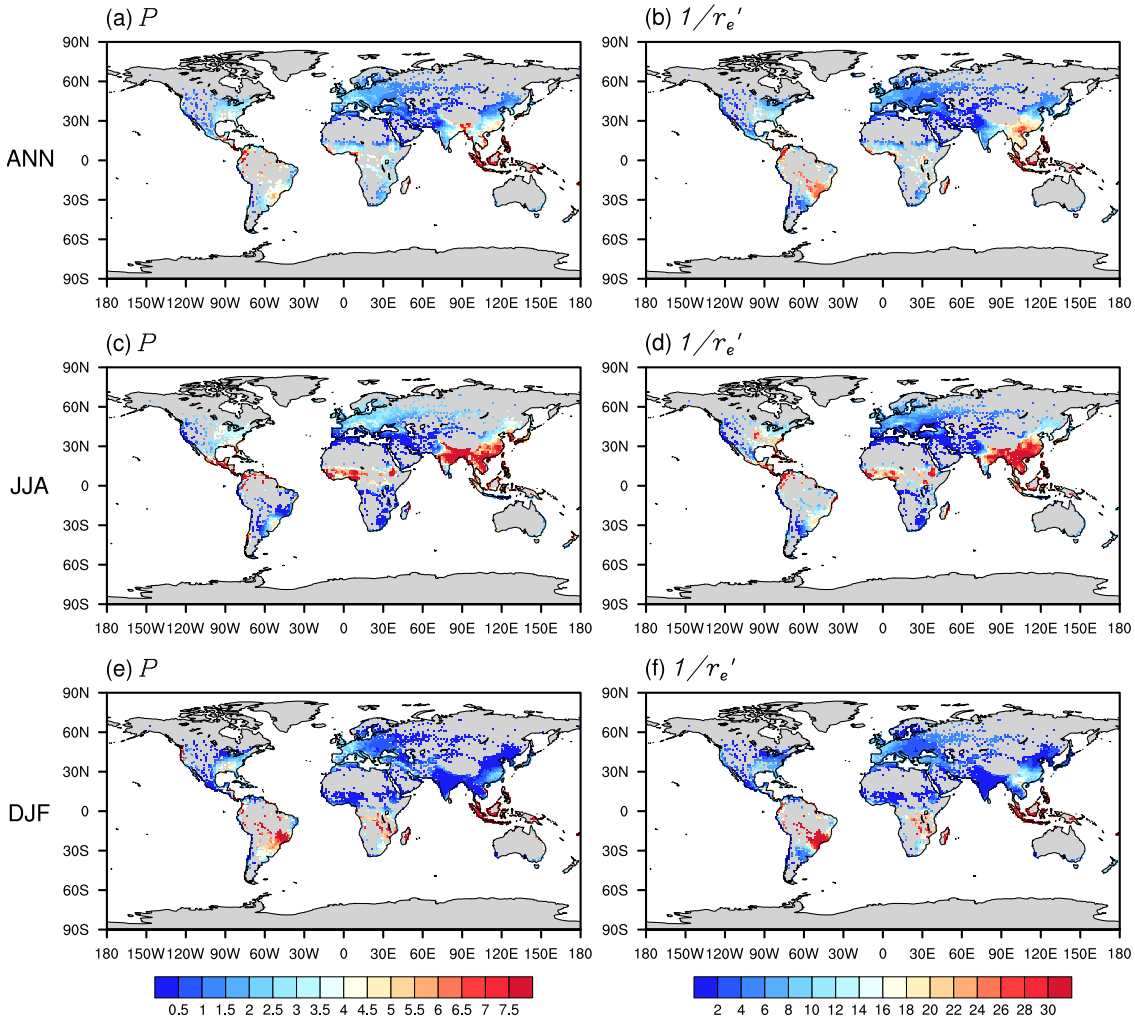

Figure S7. The spatial patterns of (a, c, e) precipitation and (b, d, f) efficiency for latent heat flux. (a-b) are the annual daily mean (ANN), (c-d) are the JJA daily mean, and (e-f) are the DJF daily mean results over 20 years (1991-2010). The results shown here are from the Case 4 (100% cool roof with albedo value of 0.7). Only grid cells with more than 0.1% of urban land are shown.

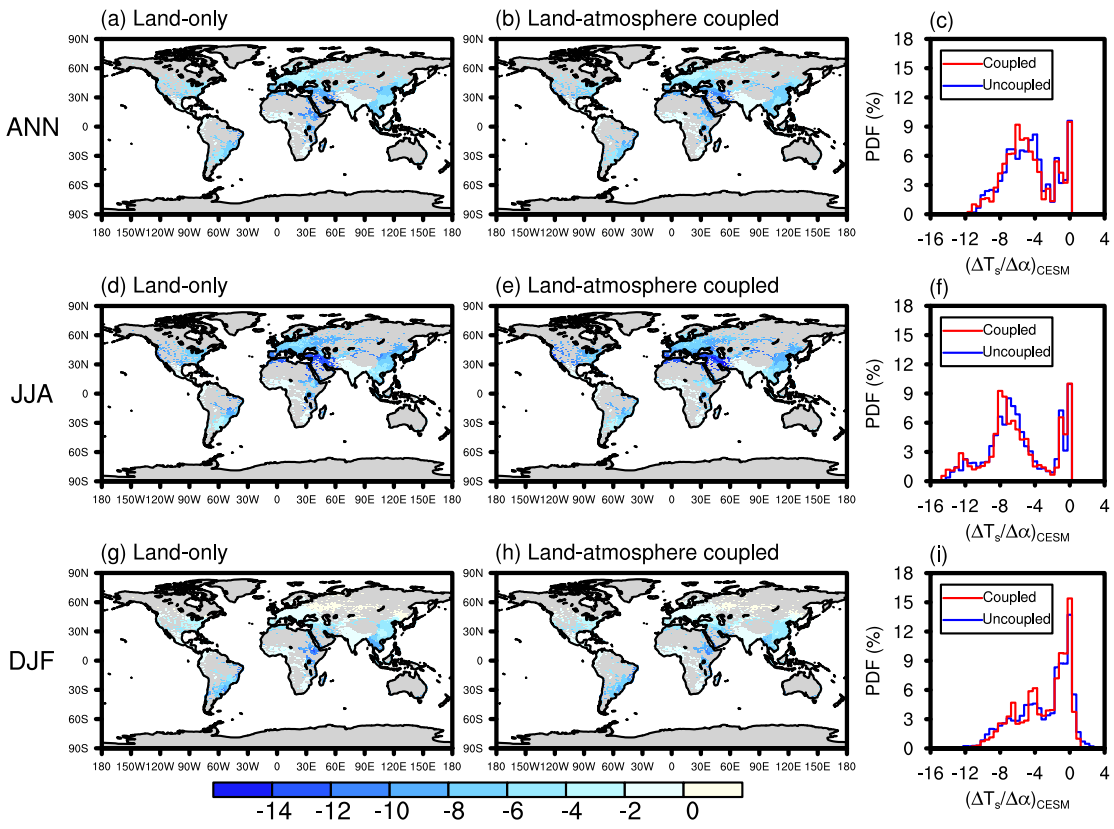

148

149 **Figure S8.** Similar to Figure S1 but comparing (a, d, g) land-only simulation (Case 4) to

150 (b, e, h) land-atmosphere coupled simulation (Case 5). (c, f, i) are the probability density

151 functions. For both land-only and land-atmosphere coupled simulations, we use 100% cool

152 roof with albedo value of 0.7.

Table S1. A list of simulations performed in this study. All simulations are conducted at a spatial resolution of 0.9° latitude by 1.25° longitude and the analysis focuses on the period 1991-2010.

	Case Names	Regular roof fraction	Cool roof fraction	Regular roof albedo	Cool roof albedo
Land-only simulations	CTL	100%	0	Varies globally according to a global dataset (Jackson et al., 2010) (see Figure S1)	0.5
	1	50%	50%		0.5
	2	50%	50%		0.7
	3	0	100%		0.5
	4	0	100%		0.7
Land-atmosphere coupled simulations	5	0	100%		0.7

Table S2. Pearson correlation coefficients computed from Case 5.

Correlation coefficients	ANN	JJA	DJF
$\Delta T_s/\Delta\alpha$ and S_{in}	-0.28	-0.7	-0.53
$\Delta T_s/\Delta\alpha$ and f	-0.75	-0.86	-0.29
f and $1/r_a'$	0.26	0.02	0.25
f and $1/r_o'$	-0.12	-0.02	-0.23
f and $1/r_g'$	-0.79	-0.71	-0.74
f and $1/r_e'$	-0.65	-0.74	-0.59